Environmental Science and Pollution Research (2023) 30:4709–4720
https://doi.org/10.1007/s11356-022-22554-3

RESEARCH ARTICLE

Facile fabrication of a 2D/2D CoFe-LDH/g-C_3N_4 nanocomposite with enhanced photocatalytic tetracycline degradation

Mengxue Li[1,2] · Mengmeng Chen[3] · Stephanie Ling Jie Lee[1,2] · Sijie Lin[1,2]

Received: 22 June 2022 / Accepted: 11 August 2022 / Published online: 16 August 2022

Abstract

The widespread use of tetracycline (TC) in medicine and agriculture has caused severe pollution problems in the environment. In this work, a nanocomposite comprising of CoFe-layered double hydroxides grown on graphitic carbon nitride nanosheets (CoFe-LDH/g-C_3N_4) with a notable two-dimensional/two-dimensional (2D/2D) heterostructure was synthesized through a facile co-precipitation method. The CoFe-LDH/g-C_3N_4 nanocomposite displayed significantly improved visible-light-driven photocatalytic activity towards TC degradation, compared to pristine g-C_3N_4 and CoFe-LDH alone. The enhanced activation efficiency was a result of intimate interfacial contact, enlarged the surface area, broadened visible-light absorbance, and enhanced photogenerated electron transfer. The scavenging experiments showed that holes (h^+) and superoxide radical anions ($\cdot O_2^-$) played a crucial role in TC degradation. Factors including the type of TCs, initial concentration of TC, presence of ions, and the type of water matrix were investigated to evaluate the practical feasibility of the nanocomposites for TC removal from antibiotics-contaminated water. The repeated tests showed that the nanocomposites possessed good stability and recyclability. This study demonstrated the feasibility of achieving photocatalytic activity enhancement of g-C_3N_4 through the formation of a 2D-2D heterostructure between LDHs and g-C_3N_4.

Keywords Layered double hydroxides · Graphitic carbon nitride · Nanocomposites · Visible-light photocatalysis · Tetracycline

Introduction

Tetracycline (TC) is an antibiotic widely used against bacterial infections in humans, veterinary medicines and agriculture (Xu et al. 2021). It has been reported that the majority of unmetabolized TC is released into natural water. TC contaminants, which are frequently detected in aquatic environments, resulted in the formation of TC-resistant bacteria and/or genes, posing adverse impacts on public health and aquatic organisms (Wang et al. 2019; Wright 2010). Accordingly, there is an urgent need to seek an effective remediation technique to remove TC from water. Traditional antibiotic removal methods (biological treatments (Yang et al. 2011), adsorption (Jia et al. 2022), membrane filtration (Ye et al. 2021)) have limited degradation ability. Semiconductor-based photocatalysis is considered a promising technique for TC removal because it can degrade contaminants into small molecules, carbon dioxide (CO_2), and water (H_2O), with the aid of solar energy (He et al. 2020; Li et al. 2022; Lin et al. 2018).

Graphite carbon nitride (g-C_3N_4), as a layered two-dimensional (2D) semiconductor, has aroused great interest in the area of photocatalysis due to its appropriate bandgap (~2.7 eV), low manufacturing cost, physicochemical stability, and non-toxicity (i.e. metal free) (Pattanayak et al. 2022; Qin et al. 2022). However, pristine g-C_3N_4 is still constrained by unsatisfactory photocatalytic activity due to its small active surface areas, restricted visible-light

Responsible Editor: Sami Rtimi

✉ Sijie Lin
lin.sijie@tongji.edu.cn

[1] College of Environmental Science and Engineering, Biomedical Multidisciplinary Innovation Research Institute, Shanghai East Hospital, Tongji University, 1239 Siping Road, Shanghai 200092, China

[2] Key Laboratory of Yangtze River Water Environment, Shanghai Institute of Pollution Control and Ecological Security, Tongji University, Shanghai 200092, China

[3] College of Environmental and Chemical Engineering, Shanghai University of Electric Power, Shanghai 200090, China

utilization, and the rapid recombination of the photoexcited carriers. The 2D-layered structure of g-C_3N_4 provides versatile possibilities of either modification or combination with other components. Recently, studies have demonstrated that the construction of 2D/2D heterojunctions (NiAl-LDH/g-C_3N_4 (Yang et al. 2022), MXene/g-C_3N_4 (Yu et al. 2021a), WO_3/g-C_3N_4 (Fu et al. 2019), black phosphorous/g-C_3N_4 (Zhang et al. 2019)) via integration of g-C_3N_4 nanosheets with other 2D semiconductors is a promising approach for g-C_3N_4 modification. This is because a 2D/2D heterojunction has a larger contact interface than zero-dimensional/two-dimensional (0D/2D) and one-dimensional/two-dimensional (1D/2D) heterojunctions, which promotes the formation of large quantities of charge transfer channels, and maximizes the transmission of photogenerated carriers. Furthermore, the interfacial bonds in a 2D/2D heterojunction can also optimize surface areas and visible-light absorbance of g-C_3N_4 (Chen et al. 2022; Xu et al. 2022).

Layered double hydroxides (LDHs) are an emerging class of 2D-layered semiconductors with unique properties, such as high specific surface areas, high thermal stability, and adjustable composition (Evans and Duan 2006, Li et al. 2020a). The formula of LDHs is usually expressed as $[M^{II}_{1-x}M^{III}_{x}(OH)_2]^{x+}(A^{y-})_{x/y}\cdot zH_2O$, where divalent M^{II} and trivalent M^{III} are metal cations (Ni^{2+}, Co^{2+}, Zn^{2+}, Fe^{3+}, Al^{3+}) and A^{n-} is the interlayer anion. Studies have shown that LDHs and their derivatives have been extensively studied in the field of adsorbents, photocatalysts, and electrocatalysts (Goh et al. 2008; Tian et al. 2022). Thus, the combination of LDHs and g-C_3N_4 to form LDHs/g-C_3N_4 2D/2D heterostructures is considered a promising strategy to enhance the photocatalytic activity of g-C_3N_4. Different types of LDHs/g-C_3N_4 composites (calcined CoFe-LDH/g-C_3N_4 (Ou et al. 2020), NiFe-LDH/g-C_3N_4 (Yan et al. 2021), CuTi-LDH/g-C_3N_4 (Guru et al. 2021), ZnAl-LDH/g-C_3N_4 (Li et al. 2020b), calcined MgZnAl-LDH/g-C_3N_4 (Yu et al. 2021b), CoZnAl-LDH/g-C_3N_4 (Yang et al. 2019b)) were explored as efficient photocatalysts for the removal of organic pollutants (antibiotics, dyes, and phenols), hexavalent chromium (VI) reduction, CO_2 reduction, hydrogen evolution, and water splitting. To our knowledge, many strategies (a hydrothermal method, a hydrothermal method/calcination, co-precipitation/calcination, self-assembly of LDHs and g-C_3N_4) involving high energy consumption and multiple steps have been used to construct the 2D/2D LDHs/g-C_3N_4 composites (Song et al. 2019). However, research on facile synthesis of LDHs/g-C_3N_4 photocatalysts is limited. Co and Fe are effective transition metals which can contribute towards structural stability of the composites and enhance the photocatalytic performance of g-C_3N_4 (Ou et al. 2020). Hence, it is of great interest to construct a CoFe-LDH/g-C_3N_4 composite via a facile synthesis method for TC removal. Additionally, study of potential applications of the composite in TC removal and elucidation of the possible photocatalysis mechanism is needed.

This work aims to explore the preparation of a CoFe-LDH/g-C_3N_4 composite with CoFe-LDH growing on g-C_3N_4 nanosheets through a facile co-precipitation method. The extent of TC removal will be used to investigate the extent of enhancement of photocatalysis under visible light. Furthermore, degradation of different types of TC, and the effects of several factors (the initial TC concentration, the presence of co-existing ions, and different water sources) on TC degradation were investigated. Regeneration of the composite was also conducted to assess the practical feasibility. The photocatalytic mechanism for TC degradation was also proposed. This work provides a facile strategy to modify 2D g-C_3N_4 with 2D LDHs and facilitates the application of LDHs/g-C_3N_4 photocatalysts for remediation of antibiotics-contaminated water.

Materials and methods

Chemicals

Tetracycline (TC), cobaltous nitrate hexahydrate ($Co(NO_3)_2\cdot 6H_2O$), iron nitrate nonahydrate ($Fe(NO_3)_3\cdot 9H_2O$), sodium hydroxide (NaOH), and salicylic acid were purchased from Shanghai Sinopharm Chemical Reagent Co., Ltd., China. Urea was acquired from Shanghai Macklin Biochemical Co., Ltd., China. All the chemicals were used directly with no further purification. Ultrapure water was used in all tests.

Synthesis of g-C_3N_4

g-C_3N_4 was fabricated using a similar method as reported previously (Scheme 1) (Zhou et al. 2019). Typically, urea and salicylic acid (98:2 wt%) were mixed into 33% ethanol solution (V/V) for 2 h and then dried. Subsequently, the dried mixture was heated at 550℃ (5 °C/min) for 2 h in a muffle furnace. After cooling down to room temperature, g-C_3N_4 was obtained and ground for further use.

Synthesis of CoFe-LDH/g-C_3N_4

CoFe-LDH/g-C_3N_4 was synthesized by a facile co-precipitation method (Scheme 1). The 1 mmol $Co(NO_3)_2\cdot 6H_2O$, 0.5 mmol $Fe(NO_3)_3\cdot 9H_2O$, and 0.2 g g-C_3N_4 were mixed in 25 mL ultrapure water, and the slurry was ultrasound treated for 0.5 h. Subsequently, the above slurry was added into 25 mL NaOH solution (3 mmol) and aged at 80℃ for 18 h. The product was then centrifuged, washed twice with ultrapure water, and freeze-dried. CoFe-LDH was synthesized under the same conditions without using g-C_3N_4.

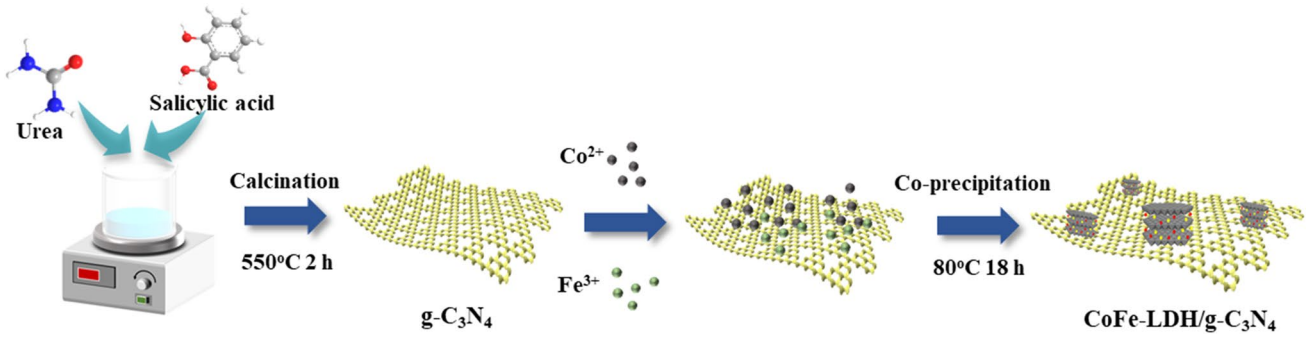

Scheme 1 Schematic diagram of the CoFe-LDH/g-C_3N_4 nanocomposites syntheses

Characterization methods

Characterization of X-ray diffraction (XRD) patterns was carried out at $2\theta = 10–70^{o}$ with Cu Kα as the radiation source (Rigaku, Ultimate IV, Japan). The Fourier transform infrared (FT-IR) spectrophotometer was recorded on Thermo Fisher Scientific Nicolet iS5 FT-IR spectrometer from 400 to 4000 cm^{-1}. The morphology and lattice structural information of materials was observed using scanning electron microscopy (SEM) (Zeiss, Sigma 300, Germany), transmission electron microscopy (TEM), and high-resolution TEM (HRTEM) (FEI, Tecnai TF20, USA). The surface area characterization was carried out by the BET measurements using the ASAP2460 instrument. X-ray photoelectron spectroscopy (XPS) measurements were collected using an XPS instrument (Thermo Fisher Scientific, K-alpha, USA). UV–Vis diffuse reflectance spectra (DRS) were obtained in the range of 200–800 nm (UV-3600, Japan). The photocurrent was conducted on a CHI-760E workstation with a three-electrode system. The degree of TC mineralization was investigated via total organic carbon (TOC) removal by a TOC-LCPH instrument (Shimadzu, Japan). The active radicals were measured by electron spin resonance (ESR) (Bruker E500) under visible-light irradiation.

Photocatalytic experiments

Photocatalytic tests for TC (40 mg/L) degradation were performed using CoFe-LDH, g-C_3N_4, and CoFe-LDH/g-C_3N_4 under 5 W LED light ($\lambda > 420$ nm). Twenty milligrams of CoFe-LDH/g-C_3N_4 were added to 40 mL of TC solution. Then, the mixture was magnetically stirred for 0.5 h in dark to attain the adsorption/desorption equilibrium. Afterward, the solution was exposed to visible-light illumination for 3 h. One millilter of suspension was extracted at varied time intervals and filtered with a 0.22-μm filter membrane. The removal of TC was determined based on the absorption at 357 nm using a Thermo Fisher Scientific microplate reader (Varioskan LUX, USA) (Tang et al. 2022). All the tests were done in duplicate.

Results and discussion

Characterization

The XRD patterns of g-C_3N_4, CoFe-LDH and CoFe-LDH/g-C_3N_4 were shown in Fig. 1a. For pure g-C_3N_4, two typical reflections at 13.1° and 27.4° corresponding to (100) and (002) crystalline planes were obtained. The (002) and (100) diffraction peaks were due to the stacking peak of aromatic system and the in-plane structure of tri-s-triazine motifs respectively (Dong et al. 2018). CoFe-LDH displayed characteristic peaks at the 2θ values of 11.5°, 24.0°, 30.8°, 36.2°, 44.2°, 58.8°, and 64.4°, which were indexed as (003), (006), (012), (015), (018), (110), and (113) planes of CoFe-LDH (Ma et al. 2020; Yang et al. 2019a). The characteristic diffraction peaks of g-C_3N_4 and CoFe-LDH were observed in the diffraction patterns of CoFe-LDH/g-C_3N_4, indicating that the crystal phases of g-C_3N_4 and CoFe-LDH exist in the nanocomposite.

Figure 1b depicted the FT-IR spectra of as-prepared g-C_3N_4, CoFe-LDH and CoFe-LDH/g-C_3N_4. For g-C_3N_4, the band at 814 cm^{-1} belonged to the characteristic breathing mode of triazine ring and the bands at 1200–1700 cm^{-1} represented the distinctive stretch modes of C-N and C=N heterocycles (Zhao et al. 2021). The bands at 3000–3500 cm^{-1} of g-C_3N_4 corresponded to N–H vibration. As for the CoFe-LDH curve, the bands which appeared at 3425 cm^{-1} and 1630 cm^{-1} were due to the stretching vibrations generated by –OH and H–O-H groups, respectively (Liu et al. 2018). The peak at 1382 cm^{-1} was assigned to the stretching mode of NO_3^-. In addition, the bands < 750 cm^{-1} were due to metal oxygen (Co–O/Fe–O) vibration modes. It could be noted that the characteristic bands of CoFe-LDH and g-C_3N_4 coexisted in the FT-IR spectra of CoFe-LDH/g-C_3N_4,

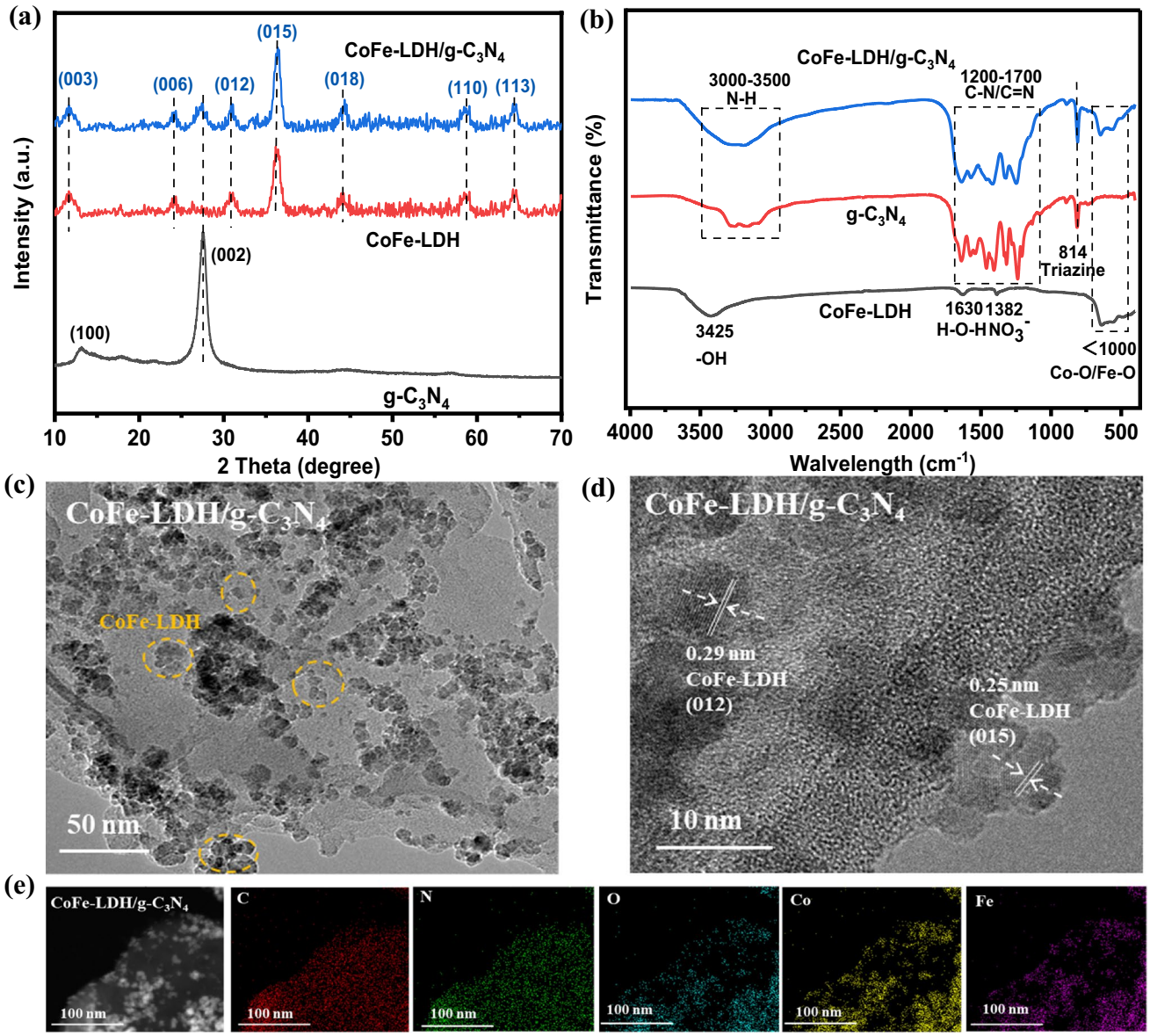

Fig. 1 **a** XRD patterns and **b** FT-IR spectra of as-prepared g-C_3N_4, CoFe-LDH and CoFe-LDH/g-C_3N_4; **c** TEM, **d** HRTEM, and **e** TEM-EDS mapping images of CoFe-LDH/g-C_3N_4

demonstrating successful synthesis of the CoFe-LDH/g-C_3N_4 nanocomposite.

The morphologies of g-C_3N_4 and CoFe-LDH/g-C_3N_4 were characterized by SEM. The SEM image for original g-C_3N_4 yielded a smooth sheet like morphology with a porous surface (Fig. S1a). After CoFe-LDH loading, CoFe-LDH/g-C_3N_4 was made up of stacked layers with rough surfaces and a jumble of nanoparticles, formed by loading of CoFe-LDH particles onto the surfaces of g-C_3N_4 during the synthesis process (Fig. S1b). TEM and HRTEM were also performed to understand the morphology and crystal lattices of CoFe-LDH/g-C_3N_4. As demonstrated in Fig. 1c, it was found that CoFe-LDH nanosheets were attached to the surface and edge of g-C_3N_4 nanosheets. The HRTEM image of the CoFe-LDH/g-C_3N_4 further proved that the interplanar spacings of 0.29 and 0.25 nm matched the (012) and (015) lattice planes of CoFe-LDH, indicating successful loading of CoFe-LDH on the g-C_3N_4 nanosheets (Fig. 1d). The EDS element mapping images of CoFe-LDH/g-C_3N_4 showed the uniform distribution of C, N, O, Co and Fe elements (Fig. 1e), confirming successful fabrication of CoFe-LDH/g-C_3N_4 heterojunctions.

BET was measured to quantify the specific surface areas, pore volumes, and pore sizes of the fabricated photocatalysts (Table 1). The specific surface areas of g-C_3N_4, CoFe-LDH, and CoFe-LDH/g-C_3N_4 were 49.34, 176.4, and 88.24 m^2/g

Table 1 The specific surface areas, pore volumes, and pore sizes of fabricated g-C_3N_4, CoFe-LDH and CoFe-LDH/g-C_3N_4

Sample	Specific surface area (m^2/g)	Pore volume (cm^3/g)	Pore size (nm)
g-C_3N_4	49.34	0.19	17.8
CoFe-LDH	176.4	0.17	3.92
CoFe-LDH/g-C_3N_4	88.24	0.24	11.04

respectively. This phenomenon indicated that the modification of CoFe-LDH could optimize the surface area of g-C_3N_4. Similarly, the pore volume of CoFe-LDH/g-C_3N_4 also increased correspondingly. In addition, the pore sizes of fabricated photocatalysts ranged from 3.92 to 17.8 nm, indicating the mesoporous property of the nanocomposites.

The elemental composition and states of the CoFe-LDH/g-C_3N_4 nanocomposite were elucidated via XPS analysis. As shown in Fig. 2a, the existence of C, N, O, Co, and Fe elements could be clearly seen in the survey spectra, revealing the presence of CoFe-LDH and g-C_3N_4 in the nanocomposite. The C 1 s spectrum exhibited three peaks at 284.5, 286.1, and 288.1 eV, belonging to C–C bond, C-O bond, and sp^2-bonded carbon (N–C = N) respectively (Fig. 2b). The three main peaks at 398.5, 400.3, and 401.2 eV shown in the N 1 s high-resolution spectra (Fig. 2c) could be assigned to sp^2-hybridized nitrogen (C = N–C), N-$(C)_3$, and C-N–H groups respectively. The O 1 s peaks located at 529.8 and 531.8 eV (Fig. 2d) arose from the metal oxygen (Co–O and Fe–O), and OH groups respectively (Gandamalla et al. 2021). As for Co 2p (Fig. 2e), the spectra was divided into Co $2p_{3/2}$ (780.4 eV) and Co $2p_{1/2}$ (795.5 eV) accompanied by two satellite peaks at 785.6 and 803.2 eV, representative of a high-spin Co^{2+} (Ou et al. 2020). As for Fe 2p (Fig. 2f), the peaks of 711.2 and 724.5 eV corresponded to Fe $2p_{3/2}$ and Fe $2p_{1/2}$, and the satellite peak at 716.5 eV was due to Fe^{3+} species (Sakita et al. 2018).

The optical absorption characteristics of the samples were studied by UV–Vis DRS (Fig. 3a). The light absorption edges appeared at 462 and 554 nm for g-C_3N_4 and CoFe-LDH/g-C_3N_4 respectively. Compared with g-C_3N_4, the absorption edge of CoFe-LDH/g-C_3N_4 was redshifted, corresponding to the narrowed bandgap (Liu et al. 2021b). It confirmed that integration of CoFe-LDH and g-C_3N_4 apparently broadened the response range of visible light which is beneficial for enhancement of the visible-light-driven photocatalytic application (Tayyab et al. 2022; Xia et al. 2019). Additionally, the bandgap energy (E_g) of g-C_3N_4 and CoFe-LDH/g-C_3N_4 were calculated based on the UV–Vis DRS and the calculation equation ($\alpha h\upsilon = A(h\upsilon - Eg)^{n/2}$). As shown in

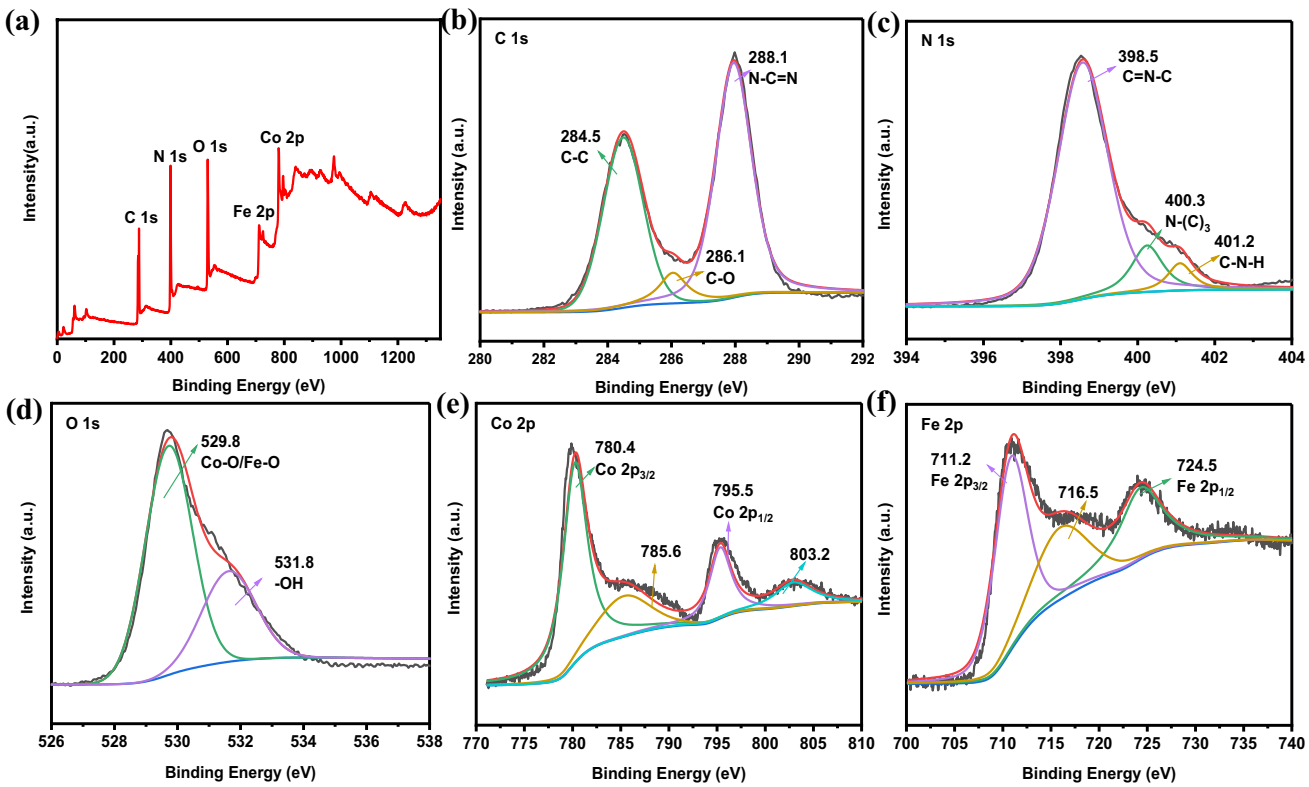

Fig. 2 XPS spectra of CoFe-LDH/g-C_3N_4: **a** survey spectra, **b** C 1 s, **c** N 1 s, **d** O 1 s, **e** Co 2P, and **f** Fe 2p

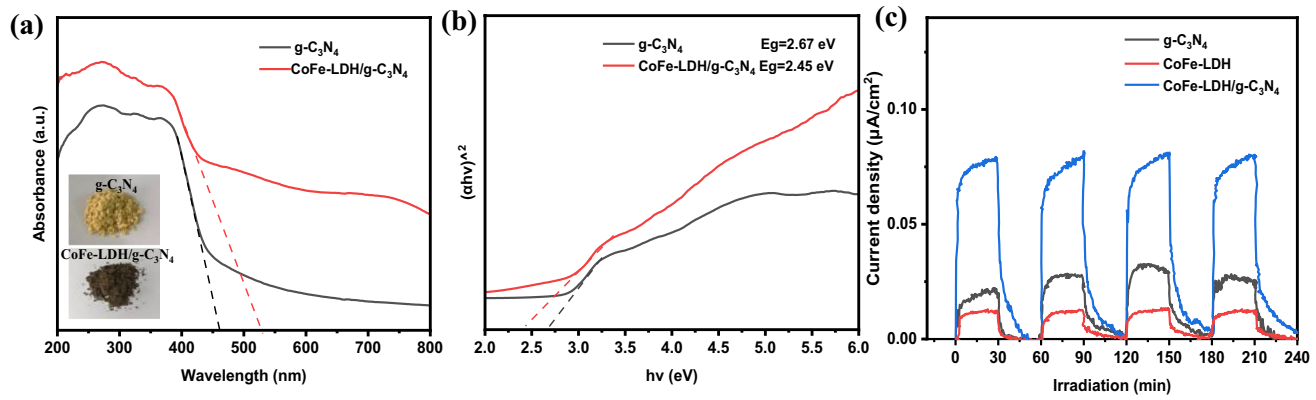

Fig. 3 **a** UV–Vis diffuse reflectance spectra, **b** the related band gap energy, and **c** transient photocurrent curves of as-prepared samples

Fig. 3b, the estimated Eg for g-C_3N_4 and CoFe-LDH/g-C_3N_4 were 2.67 and 2.45 eV respectively.

Photocurrent tests were performed to study the separation properties of photoinduced electrons and holes in the nanocomposite. Figure 3c displayed the transient photocurrent measurements of g-C_3N_4, CoFe-LDH, and CoFe-LDH/g-C_3N_4 for several light on and light off cycles under visible-light irradiation. The photocurrent response of CoFe-LDH/g-C_3N_4 was the highest among the three nanocomposites, indicating the lowest recombination of electrons and holes (Ou et al. 2020).

Photocatalytic degradation performance

The photocatalytic activity of the synthesized CoFe-LDH, g-C_3N_4 and CoFe-LDH/g-C_3N_4 for degradation of TC was evaluated under visible LED light irradiation. The adsorption/desorption equilibrium was initially investigated prior to photocatalysis (Fig. 4a). After adsorption for 0.5 h in dark, g-C_3N_4, CoFe-LDH, and CoFe-LDH/g-C_3N_4 exhibited TC removal efficiencies of about 5.1%, 40.8%, and 37.1% respectively. The enhanced adsorption capacity of CoFe-LDH/g-C_3N_4 could be due to the larger specific surface area and pore volume (Table 1).

In the absence of photocatalysts, the percentage of the TC solution under visible-light illumination did not change with time (Fig. 4b). For pure g-C_3N_4, the photodegradation efficiency was 55.0% within 3 h, whereas for pure CoFe-LDH it was 58.4%. Modification with CoFe-LDH markedly enhanced the photoactivity of g-C_3N_4. CoFe-LDH/g-C_3N_4 exhibited the highest degradation efficiency of 83.8%, which was associated with an enhanced TC adsorption capacity, extended visible-light response, and efficient charge separation. The pseudo first-order kinetic model ($ln\ (C_0/C) = kt$) was utilized to further analyze the photodegradation of TC (Fig. 4c). It could be seen that the degradation rate (k) value of CoFe-LDH/g-C_3N_4 (0.43 h^{-1}) was 1.87 and 2.26 times that of the original g-C_3N_4 and CoFe-LDH respectively. Lastly, it was worth noting that the photocatalytic performance of CoFe-LDH/g-C_3N_4 was efficient (measured as antibiotic degradation per unit mass of photocatalysts), as compared to other reported LDHs/g-C_3N_4 (Table 2).

The degree of TC mineralization was determined by the TOC removal. From Fig. 4d, it was observed that the TOC removal efficiency of CoFe-LDH/g-C_3N_4 increased with the duration of visible-light irradiation, suggesting that TC mineralization increased with longer visible-light irradiation duration. The TOC removal efficiency reached 77.7% after 3 h of treatment, which was lower than the degradation efficiency of TC owing to the formation of various intermediates and by-products.

Practicability of CoFe-LDH/g-C_3N_4

To testify the universal degradation effectiveness of the CoFe-LDH/g-C_3N_4 nanocomposite on various TC antibiotics, the removal of TC-based antibiotics was carried out based on the optimum dosage of 0.5 g/L (Text S1 and Fig. S2a). TC (tetracycline), OTC (oxytetracycline), CTC (chlortetracycline), and DTC (doxycycline) were selected as the TC-based antibiotics for testing. CoFe-LDH/g-C_3N_4 could adsorb TC (37.1%), OTC (49.4%), CTC (71.8%), and DTC (61.7%) at an initial concentration of 40 mg/L (Fig. 5a). Of TC, OTC, CTC, and DTC, 83.8%, 77.5%, 91.3%, and 89.1% respectively were subsequently degraded within 3 h, through CoFe-LDH/g-C_3N_4 photocatalysis, indicating excellent degradation of TCs over CoFe-LDH/g-C_3N_4.

Considering that concentrations of TC in natural water vary under different circumstances (pharmaceutical institutions effluents, medical factories, and untreated domestic sewage) (Chen et al. 2018; Kummerer 2002), the effects of various initial TC concentrations on TC removal efficiency over CoFe-LDH/g-C_3N_4 were investigated. The degradation efficiencies of TC exceeded 83.8% at lower TC concentration

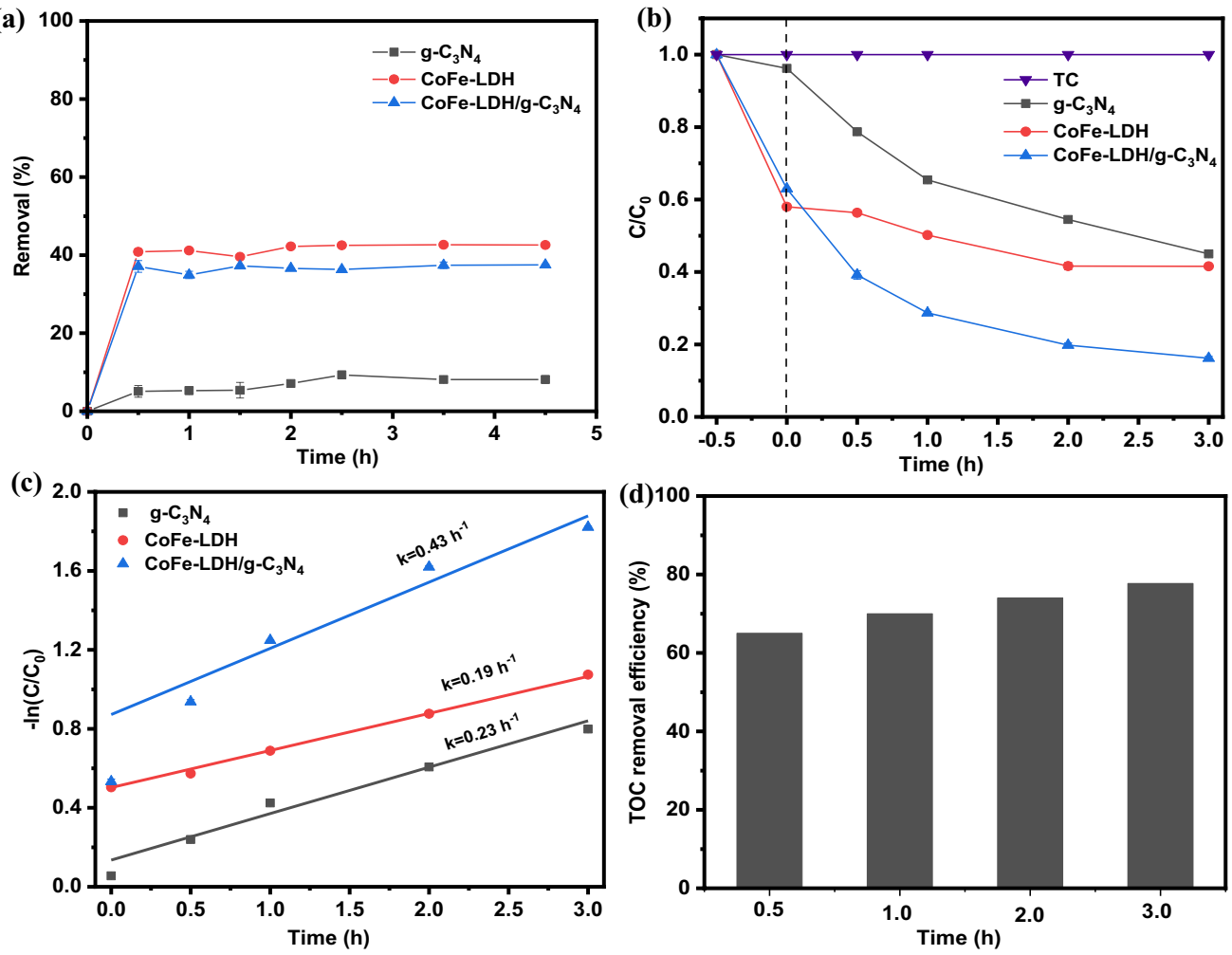

Fig. 4 **a** TC adsorption capacity; **b** adsorption and photocatalysis capacity; **c** kinetics analysis for TC photodegradation; **d** TOC removal efficiency by CoFe-LDH/g-C_3N_4 under visible-light irradiation

(20 and 40 mg/L) (Fig. 5b), proving that application of CoFe-LDH/g-C_3N_4 to natural water containing low TC concentrations was feasible. CoFe-LDH/g-C_3N_4 retained a TC degradation efficiency of 49.7% (Fig. 5b) at the high TC concentration (100 mg/L), indicating potential applications for treatment of water contaminated with high concentrations of TC.

Because of the presence of large number of inorganic ions and organic substances in natural water, it is necessary to discuss their effects on photocatalysis. Various anions (Cl^-, SO_4^{2-}, $H_2PO_4^-$, and CO_3^{2-}) at the concentration of 10 mg/L were employed to investigate the influences of ion interference. The anions caused inhibition effects on TC degradation efficiencies in the order: $Cl^- < CO_3^{2-} < SO_4^{2-} < H_2PO_4^-$ (Fig. 5c). Cl^- and CO_3^{2-} exhibited minimal effects on TC degradation. A slight enhancement of the reaction rate (k) was found in the presence of Cl^-, which may be attributed to the scavenging activity of the photogenerated holes and Cl^-, resulting in more effective separation of electrons and holes (Xu et al. 2018). It is known that adding $H_2PO_4^-$ can lower solution pH (Abdelhaleem and Chu 2017), which can affect the stability of the nanocomposite leading to an inhibitory effect (Li et al. 2022). Moreover, inhibitory effects in the presence of $H_2PO_4^-$ and SO_4^{2-} might also be attributed to competition with TC for active sites and quenching effects on the radicals. Humic acid (HA) was used as an organic matter. As shown in Fig. S2b, the TC removal efficiency slightly decreased when HA concentration increased to 15 mg/L. This result was mainly ascribed to the fact that HA could act a role in shading and competing with TC for free radicals at higher concentrations (Wang et al. 2020).

Considering the potential application of the CoFe-LDH/g-C_3N_4 nanocomposite for treatment of antibiotic-contaminated natural water, removal of TC from different water sources was tested (Fig. 5d). The main properties

Table 2 Comparison of the photocatalytic performance of CoFe-LDH/g-C_3N_4 with other LDHs/g-C_3N_4 for antibiotic degradation

Photocatalysts	Antibiotics	Concentration (mg/L)	Dosage (g/L)	Degradation of antibiotic per unit mass of photocatalysts (mg/g)	Visible-light source	Degradation time/efficiency	Refs
NiFe-LDH/g-C_3N_4	Tetracycline hydrochloride	20	0.4	50	500 W Xe lamp	60 min, 96.8%	(Zhao et al. 2021)
Calcined MgZnAl-LDH/g-C_3N_4	Tetracycline	10	0.5	20	300 W Xe lamp	120 min, 99.0%	(Yu et al. 2021b)
ZnAl-LDH/g-C_3N_4	Ciprofloxacin	20	0.6	33	300 W Xe lamp	150 min, 84.0%	(Gandamalla et al. 2021)
ZnTi-LDH/g-C_3N_4	Ceftriaxone sodium	10	1	10	300 W Xe lamp	240 min, 97.0%	(Sun et al. 2019)
ZnCuMg-LDH/g-C_3N_4	Sulfadiazine	37.5	0.5	75	15 W LED	130 min, 93.0%	(Gholami et al. 2020)
Calcined ZnFe-LDH/g-C_3N_4	Sulfadiazine	5	0.5	10	500 W Xe lamp	240 min, ~ 100%	(Di et al. 2019)
CoAl-LDH/g-C_3N_4/GO	Tetracycline	20	0.25	80	300 W halogen lamp	60 min, 99.0%	(Jo and Tonda 2019)
CoAl-LDH/g-C_3N_4	Sulfadiazine	2.5	0.1	25	100 W/m^2	15 min, 87.1%	(Zeng et al. 2020)
CoFe-LDH/g-C_3N_4	Tetracycline	40	0.5	80	5 W LED	180 min, ~ 83.8%	**This study**

of the water sources were presented in Table S1. Compared to ultrapure water (83.8%), there was a negligible loss in the removal efficiencies of TC in drinking water (79.2%) and tap water (81.9%), whereas the removal efficiency of TC fell slightly in aquaculture water (70.6%). The decreased rate constants (k) were observed (Fig. 5d, the insert), which may be due to the effects of organic and inorganic ions present in the various water sources on TC photodegradation (Wang et al. 2018). Overall, the results showed CoFe-LDH/g-C_3N_4 showed potential for practical application.

The reusability and chemical stability of photocatalysts are associated with practical applications in water treatment. Here, the cycling degradation experiments were carried out. Before each cycle test, the nanocomposite was retrieved by rinsing with ultrapure water and drying (80 °C). The photocatalytic efficiency of CoFe-LDH/g-C_3N_4 did not display significant deterioration across three different cycles, and ~ 73.6% of TC could still be removed after three cycles (Fig. 5e), indicating that the CoFe-LDH/g-C_3N_4 possessed good photocatalytic stability. Meanwhile, the crystal structures of the fresh and used nanocomposites were compared using XRD analysis (Fig. 5f). Compared with the fresh nanocomposite, the peak intensity of the used nanocomposite was slightly reduced, which may be due to the unavoidable loss of ordered structure during photocatalysis. In spite of this, the overall crystal structure of recycled CoFe-LDH/g-C_3N_4 was almost identical to that of the fresh one, implying high chemical stability.

The possible photocatalytic mechanism

The roles of the main reactive substances were determined to reveal the mechanism involved in TC degradation over CoFe-LDH/g-C_3N_4. The scavengers (1 mM) of benzoquinone (BQ), isopropanol (IPA), and ethylenediaminetetraacetic acid disodium (EDTA-2Na) were used to quench superoxide radical anions (O_2^-), hydroxyl radicals (OH), and holes (h^+) respectively (Li et al. 2022; Liu et al. 2021a). As shown in Fig. 6a, the degradation of TC was significantly depressed after the addition of EDTA-2Na and BQ, suggesting h^+ and·O_2^- were the main free active radical for TC degradation. Meanwhile, the removal efficiency of TC was only reduced by approximately 6.6% in the presence of IPA, which demonstrated that ·OH played a minor role in the degradation process. The generated active radicals over CoFe-LDH/g-C_3N_4 were further confirmed by ESR measurement (Fig. 6b and c). The signals of DMPO-O_2^- and DMPO-OH were not observed in dark, but were detected under visible-light irradiation. ESR results indicated that·O_2^- and·OH could be generated in the photocatalytic process over CoFe-LDH/g-C_3N_4, which was agreement with the results of quenching tests.

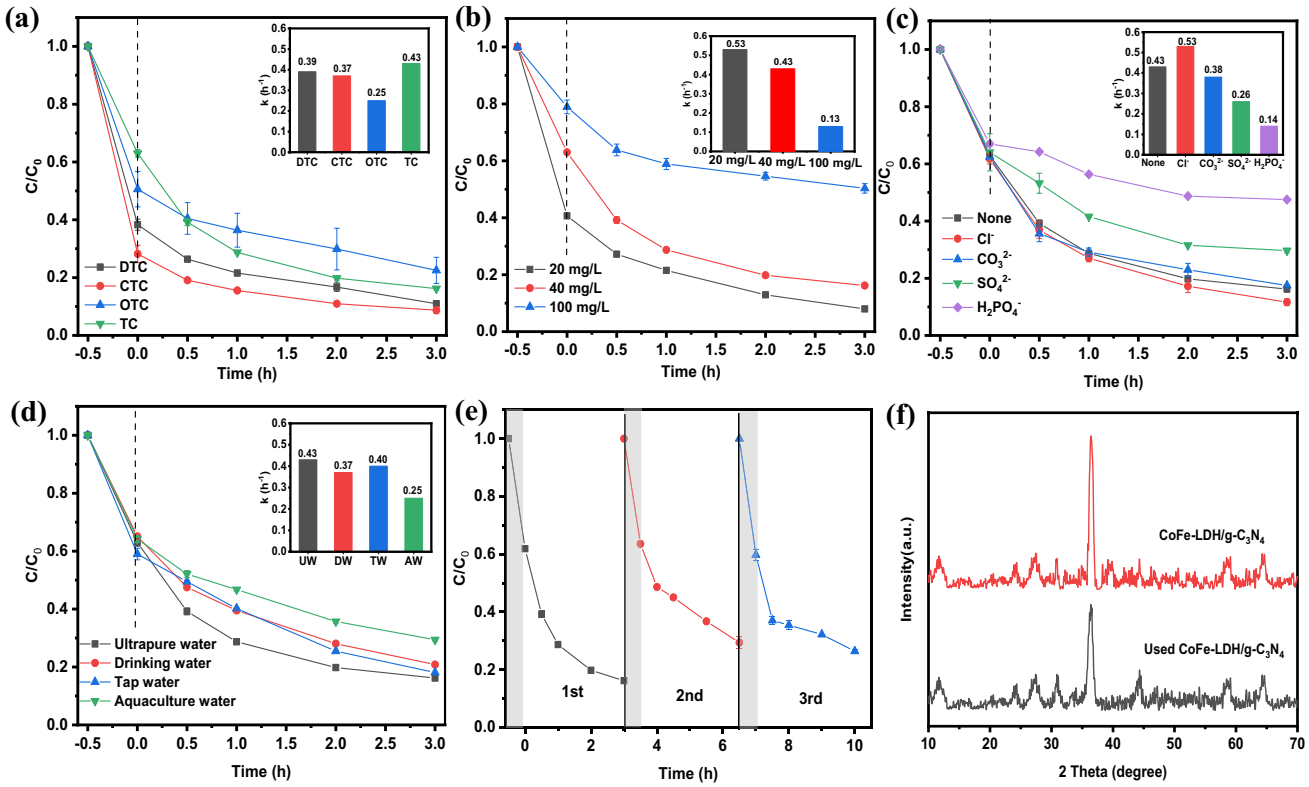

Fig. 5 Effects of **a** different TC types, **b** initial TC concentration, **c** inorganic ions, **d** various water sources on TC degradation by CoFe-LDH/g-C_3N_4 under visible light; **e** cycling runs for TC degradation using CoFe-LDH/g-C_3N_4; **f** XRD patterns of the fresh and used CoFe-LDH/g-C_3N_4

The E_g values of g-C_3N_4 and CoFe-LDH were 2.67 eV and 1.63 eV, respectively (Fig. 3b and Fig. S3). Fig. S4 showed the valance band X-ray photoelectron spectroscopy (VB-XPS) spectra of the samples. The conduction band (CB) and VB values of g-C_3N_4 were calculated to be − 0.67 and 2.0 eV, while that of CoFe-LDH were − 0.93 and 0.70 eV. The possible degradation mechanism of CoFe-LDH/g-C_3N_4 was proposed in Scheme 2 based on the above observations. Under dark condition, CoFe-LDH/g-C_3N_4 with a high surface area (88.24 m^2/g) provided enough surface sites (Table 1) and pore structures to adsorb TC, thus causing TC enrichment on the nanocomposite. CoFe-LDH/g-C_3N_4 could harvest more visible light after the introduction of LDH. Under visible-light irradiation, g-C_3N_4 and CoFe-LDH were excited to produce electrons (e^-) in the CB, resulting the generation of h^+ in the VB. The 2D/2D

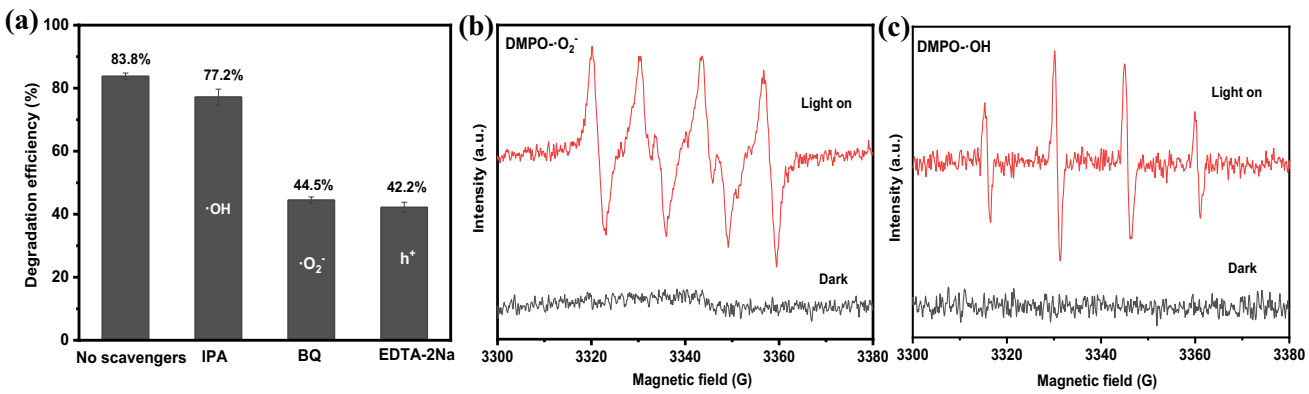

Fig. 6 **a** Photocatalytic activity of CoFe-LDH/g-C_3N_4 for TC degradation with different radical scavengers; ESR spectra of **b** DMPO-O_2^- and **c** DMPO-OH for CoFe-LDH/g-C_3N_4 in the dark and under visible-light irradiation

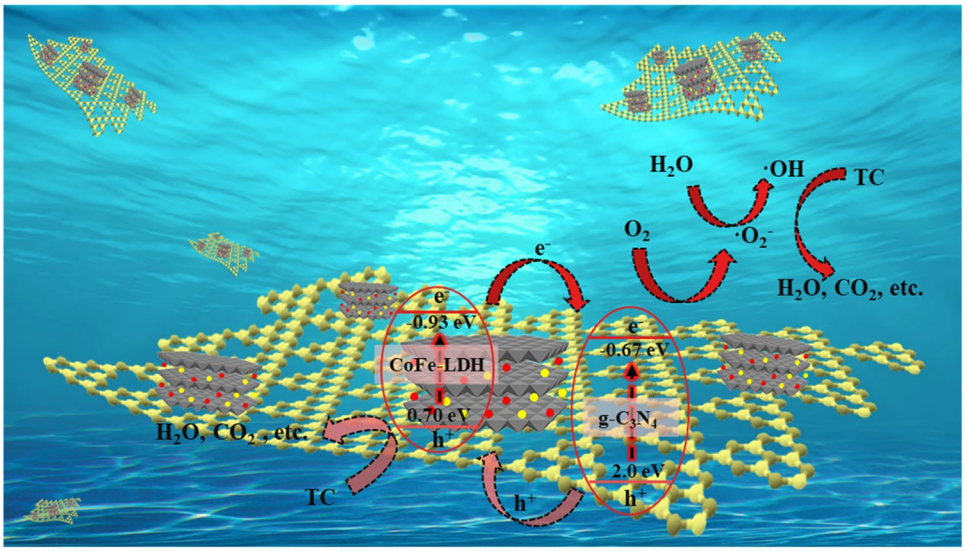

Scheme 2 Schematic diagram illustrating the possible photocatalytic mechanism for TC degradation over CoFe-LDH/g-C_3N_4 under visible-light irradiation

nanosheet architecture could shorten the diffusion path, and give rise to efficient separation and transportation of e^- and h^+. The excited e^- in the CB of CoFe-LDH may transfer to the CB of g-C_3N_4, while the produced h^+ in the VB of g-C_3N_4 may transfer to the VB of CoFe-LDH, resulting in the low recombination of the photoinduced electron–hole pairs. The accumulated e^- on g-C_3N_4 reacted with dissolved O_2 in water to produce·O_2^-, which was responsible for the degradation of TC. Meanwhile,·O_2^- reacted with H_2O and e^- to form·OH, which served as an active specie for TC degradation. The h^+ accumulated in the VB of CoFe-LDH could react directly with the TC to form H_2O, CO_2, and other small molecules.

Conclusion

In this article, a 2D/2D CoFe-LDH/g-C_3N_4 nanocomposite was prepared by introducing 2D CoFe-LDH on 2D g-C_3N_4 nanosheets through a simple co-precipitation method. The synthesized nanocomposite was used to remove TC from aqueous solutions under visible-light irradiation. CoFe-LDH/g-C_3N_4 showed efficient photocatalytic performance (achieving 83.8% of degradation within 3 h) as compared to pure g-C_3N_4 and CoFe-LDH, and even the reported LDHs/g-C_3N_4 composites. The accelerated photocatalytic activity was due to the face-to-face interfacial contact of 2D/2D heterojunction which optimized the surface area, widened visible-light absorbance, and promoted separation/migration of photogenerated carriers. Degradation of different TCs, the effects of various environmental factors (initial TC concentration, co-existing ions, and water sources) on TC degradation were studied, demonstrating the prospect of CoFe-LDH/g-C_3N_4 for practical applications. The good reusability and stability of CoFe-LDH/g-C_3N_4 were evaluated by conducting three cycle tests. h^+ and·O_2^- were the main oxidative radicals in the degradation of TC. This study offers a facile method to enhance the visible-light photocatalytic performance of g-C_3N_4 via construction of 2D/2D LDHs/g-C_3N_4 composites and facilitates photocatalytic application of LDHs/g-C_3N_4 composites.

Supplementary Information The online version contains supplementary material available at https://doi.org/10.1007/s11356-022-22554-3.

Author contribution Mengxue Li: conceptualization, investigation, methodology, writing—review and editing. Mengmeng Chen: data curation. Stephanie Ling Jie Lee: writing—review and editing. Sijie Lin: project design, supervision, writing—review and editing, project administration, funding acquisition.

Funding This work has received the financial support from the National Natural Science Foundation of China (No. 21777116) and the Fundamental Research Funds for the Central Universities.

Data availability All data generated or analyzed during the current work are included in this published article and its supplementary information files.

Declarations

Competing interests The authors declare no competing interests.

References

Abdelhaleem A, Chu W (2017) Photodegradation of 4-chlorophenoxyacetic acid under visible LED activated N-doped TiO2 and the mechanism of stepwise rate increment of the reused catalyst. J Hazard Mater 338:491–501

Chen H, Jing L, Teng Y, Wang J (2018) Characterization of antibiotics in a large-scale river system of China: occurrence pattern,

spatiotemporal distribution and environmental risks. Sci Total Environ 618:409–418
Chen M, Li M, Lee SLJ, Zhao X, Lin S (2022) Constructing novel graphitic carbon nitride-based nanocomposites - from the perspective of material dimensions and interfacial characteristics. Chemosphere 302:134889
Di G, Zhu Z, Huang Q, Zhang H, Zhu J, Qiu Y, Yin D, Zhao J (2019) Targeted modulation of g-C3N4 photocatalytic performance for pharmaceutical pollutants in water using ZnFe-LDH derived mixed metal oxides: structure-activity and mechanism. Sci Total Environ 650:1112–1121
Dong H, Guo X, Yang C, Ouyang Z (2018) Synthesis of g-C3N4 by different precursors under burning explosion effect and its photocatalytic degradation for tylosin. Appl Catal B-Environ 230:65–76
Evans DG, Duan X (2006) Preparation of layered double hydroxides and their applications as additives in polymers, as precursors to magnetic materials and in biology and medicine. Chem Commun 5:485–496
Fu J, Xu Q, Low J, Jiang C, Yu J (2019) Ultrathin 2D/2D WO3/g-C3N4 step-scheme H2-production photocatalyst. Appl Catal B-Environ 243:556–565
Gandamalla A, Manchala S, Verma A, Fu YP, Shanker V (2021) Microwave-assisted synthesis of ZnAl-LDH/g-C3N4 composite for degradation of antibiotic ciprofloxacin under visible-light illumination. Chemosphere 283:131182
Gholami P, Khataee A, Vahid B, Karimi A, Golizadeh M, Ritala M (2020) Sonophotocatalytic degradation of sulfadiazine by integration of microfibrillated carboxymethyl cellulose with Zn-Cu-Mg mixed metal hydroxide/g-C3N4 composite. Sep Purif Technol 245:116866
Goh K-H, Lim T-T, Dong Z (2008) Application of layered double hydroxides for removal of oxyanions: a review. Water Res 42:1343–1368
Guru S, Kumar S, Bellamkonda S, Gangavarapu RR (2021) Synthesis of CuTi-LDH supported on g-C3N4 for electrochemical and photoelectrochemical oxygen evolution reactions. Int J Hydrogen Energ 46:16414–16430
He Y, Peng G, Jiang Y, Zhao M, Wang X, Chen M, Lin S (2020) Environmental hazard potential of nano-photocatalysts determined by nano-bio interactions and exposure conditions. Small 16:e1907690
Jia F, Zhao D, Shu M, Sun F, Wang D, Chen C, Deng Y, Zhu X (2022) Co-doped Fe-MIL-100 as an adsorbent for tetracycline removal from aqueous solution. Environ Sci Pollut R 29:55026–55038
Jo WK, Tonda S (2019) Novel CoAl-LDH/g-C3N4/RGO ternary heterojunction with notable 2D/2D/2D configuration for highly efficient visible-light-induced photocatalytic elimination of dye and antibiotic pollutants. J Hazard Mater 368:778–787
Kummerer K (2002) Drugs in the environment: emission of drugs, diagnostic aids and disinfectants into wastewater by hospitals in relation to other sources - a review (vol 45, pg 957, 2001). Chemosphere 48:383–383
Li M, Li L, Lin S (2020a) Efficient antimicrobial properties of layered double hydroxide assembled with transition metals via a facile preparation method. Chinese Chem Lett 31:1511–1515
Li M, Li P, Zhang L, Chen M, Tang J, Qin C, Ling Jie Lee S, Lin S (2022) Facile fabrication of ZnO decorated ZnFe-layered double hydroxides @ biochar nanocomposites for synergistic photodegradation of tetracycline under visible light. Chem Eng J 434:134772
Li X, Yu Z, Shao L, Zeng H, Liu Y, Feng X (2020b) A novel strategy to construct a visible-light-driven Z-scheme (ZnAl-LDH with active phase/g-C3N4) heterojunction catalyst via polydopamine bridge (a similar "bridge" structure). J Hazard Mater 386:121650
Lin S, Yu T, Yu Z, Hu X, Yin D (2018) Nanomaterials safer-by-design: an environmental safety perspective. Adv Mater 30:e1705691
Liu G, Feng M, Tayyab M, Gong J, Zhang M, Yang M, Lin K (2021a) Direct and efficient reduction of perfluorooctanoic acid using bimetallic catalyst supported on carbon. J Hazard Mater 412:125224
Liu J, Li J, Wang L, Bing X, Cui X, Ji F, Dienguila Kionga D (2018) Synthesis of a novel magnetic SnNb2O6/CoFe-LDH 2D/2D heterostructure for the degradation of organic pollutants under visible light irradiation. J Mater Sci 54:172–187
Liu Y, Zhu Q, Tayyab M, Zhou L, Lei J, Zhang J (2021b) Single-atom Pt loaded zinc vacancies ZnO–ZnS induced type-V electron transport for efficiency photocatalytic H2 evolution. Solar RRL 5:2100536
Ma Q, Nengzi L-c, Li B, Wang Z, Liu L, Cheng X (2020) Heterogeneously catalyzed persulfate with activated carbon coated with CoFe layered double hydroxide (AC@ CoFe-LDH) for the degradation of lomefloxacin. Sep Purif Technol 235:116204
Ou B, Wang J, Wu Y, Zhao S, Wang Z (2020) Efficient removal of Cr (VI) by magnetic and recyclable calcined CoFe-LDH/g-C3N4 via the synergy of adsorption and photocatalysis under visible light. Chem Eng J 380:122600
Pattanayak DS, Pal D, Mishra J, Thakur C, Wasewar KL (2022) Doped graphitic carbon nitride (g-C3N4) catalysts for efficient photodegradation of tetracycline antibiotics in aquatic environments. Environ Sci Pollut R (in press)
Qin C, Tang J, Qiao R, Lin S (2022) Tetracycline sensitizes TiO2 for visible light photocatalytic degradation via ligand-to-metal charge transfer. Chinese Chem Lett 33:5218–5222
Sakita AMP, Noce RD, Vallés E, Benedetti AV (2018) Pulse electrodeposition of CoFe thin films covered with layered double hydroxides as a fast route to prepare enhanced catalysts for oxygen evolution reaction. Appl Surf Sci 434:1153–1160
Song B, Zeng Z, Zeng G, Gong J, Xiao R, Ye S, Chen M, Lai C, Xu P, Tang X (2019) Powerful combination of g-C3N4 and LDHs for enhanced photocatalytic performance: a review of strategy, synthesis, and applications. Adv Colloid Interface Sci 272:101999
Sun D, Chi D, Yang Z, Xing Z, Yin J, Li Z, Zhu Q, Zhou W (2019) Mesoporous g-C3N4/Zn–Ti LDH laminated van der Waals heterojunction nanosheets as remarkable visible-light-driven photocatalysts. Int J Hydrogen Energ 44:16348–16358
Tang J, Wang J, Tang L, Feng C, Zhu X, Yi Y, Feng H, Yu J, Ren X (2022) Preparation of floating porous g-C3N4 photocatalyst via a facile one-pot method for efficient photocatalytic elimination of tetracycline under visible light irradiation. Chem Eng J 430:132669
Tayyab M, Liu Y, Min S, Muhammad Irfan R, Zhu Q, Zhou L, Lei J, Zhang J (2022) Simultaneous hydrogen production with the selective oxidation of benzyl alcohol to benzaldehyde by a noble-metal-free photocatalyst VC/CdS nanowires. Chinese J Catal 43:1165–1175
Tian Y, Li S, Huang R, Wei Z, Ji X, Liu P, Li Y, Jing Q (2022) Rational construction of core-branch Co3O4@ CoNi-layered double hydroxide nanoarrays as efficient electrocatalysts for oxygen evolution reaction. J Alloy Compd 899:163259
Wang H, Wu Y, Feng M, Tu W, Xiao T, Xiong T, Ang H, Yuan X, Chew JW (2018) Visible-light-driven removal of tetracycline antibiotics and reclamation of hydrogen energy from natural water matrices and wastewater by polymeric carbon nitride foam. Water Res 144:215–225
Wang Y, Yin Z, Zhao H, Hu J, Kang Y (2019) The effects of tetracycline concentrations on tetracycline resistance genes and their bacterial hosts in the gut passages of earthworms (*Eisenia fetida*) feeding on domestic sludge. Environ Sci Pollut R 26:34412–34420
Wang Y, Rao L, Wang P, Shi Z, Zhang L (2020) Photocatalytic activity of N-TiO2/O-doped N vacancy g-C3N4 and the intermediates toxicity evaluation under tetracycline hydrochloride and Cr (VI) coexistence environment. Appl Catal B-Environ 262:118308

Wright GD (2010) Antibiotic resistance in the environment: a link to the clinic? Curr Opin Microbiol 13:589–594

Xia D, Liu H, Xu B, Wang Y, Liao Y, Huang Y, Ye L, He C, Wong PK, Qiu R (2019) Single Ag atom engineered 3D-MnO2 porous hollow microspheres for rapid photothermocatalytic inactivation of E. coli under solar light. Appl Catal B-Environ 245:177–189

Xu L, Yang L, Johansson EM, Wang Y, Jin P (2018) Photocatalytic activity and mechanism of bisphenol a removal over TiO2−x/rGO nanocomposite driven by visible light. Chem Eng J 350:1043–1055

Xu L, Zhang H, Xiong P, Zhu Q, Liao C, Jiang G (2021) Occurrence, fate, and risk assessment of typical tetracycline antibiotics in the aquatic environment: a review. Sci Total Environ 753:141975

Xu Z, Shi Y, Li L, Sun H, Amin MS, Guo F, Wen H, Shi W (2022) Fabrication of 2D/2D Z-scheme highly crystalline carbon nitride/δ-Bi2O3 heterojunction photocatalyst with enhanced photocatalytic degradation of tetracycline. J Alloy Compd 895:162667

Yan J, Zhang X, Zheng W, Lee LYS (2021) Interface engineering of a 2D–C3N4/NiFe-LDH heterostructure for highly efficient photocatalytic hydrogen evolution. ACS Appl Mater Interfaces 13:24723–24733

Yang M, Wang P, Li Y, Tang S, Lin X, Zhang H, Zhu Z, Chen F (2022) Graphene aerogel-based NiAl-LDH/g-C3N4 With ultratight sheet-sheet heterojunction for excellent visible-light photocatalytic activity of CO_2 reduction. Appl Catal B-Environ 306:121065

Yang R, Zhou Y, Xing Y, Li D, Jiang D, Chen M, Shi W, Yuan S (2019a) Synergistic coupling of CoFe-LDH arrays with NiFe-LDH nanosheet for highly efficient overall water splitting in alkaline media. Appl Catal B-Environ 253:131–139

Yang S-F, Lin C-F, Lin AY-C, Hong P-KA (2011) Sorption and biodegradation of sulfonamide antibiotics by activated sludge: experimental assessment using batch data obtained under aerobic conditions. Water Res 45:3389–3397

Yang Y, Wu J, Xiao T, Tang Z, Shen J, Li H, Zhou Y, Zou Z (2019b) Urchin-like hierarchical CoZnAl-LDH/RGO/g-C3N4 hybrid as a Z-scheme photocatalyst for efficient and selective CO_2 reduction. Appl Catal B-Environ 255:117771

Ye J, Li C, Wang L, Wang Y, Dai J (2021) Synergistic multiple active species for catalytic self-cleaning membrane degradation of persistent pollutants by activating peroxymonosulfate. J Colloid Interf Sci 587:202–213

Yu M, Liang H, Zhan R, Xu L, Niu J (2021a) Sm-doped g-C3N4/Ti3C2 MXene heterojunction for visible-light photocatalytic degradation of ciprofloxacin. Chinese Chem Lett 32:2155–2158

Yu Y, Chen D, Xu W, Fang J, Sun J, Liu Z, Chen Y, Liang Y, Fang Z (2021b) Synergistic adsorption-photocatalytic degradation of different antibiotics in seawater by a porous g-C3N4/calcined-LDH and its application in synthetic mariculture wastewater. J Hazard Mater 416:126183

Zeng H, Zhang H, Deng L, Shi Z (2020) Peroxymonosulfate-assisted photocatalytic degradation of sulfadiazine using self-assembled multi-layered CoAl-LDH/g-C3N4 heterostructures: Performance, mechanism and eco-toxicity evaluation. J Water Process Eng 33:101084

Zhang X, Deng J, Yan J, Song Y, Mo Z, Qian J, Wu X, Yuan S, Li H, Xu H (2019) Cryo-mediated liquid-phase exfoliated 2D BP coupled with 2D C3N4 to photodegradate organic pollutants and simultaneously generate hydrogen. Appl Surf Sci 490:117–123

Zhao G-Q, Long X, Hu J, Zou J, Jiao F-P (2021) NiFe-layered double hydroxides as a novel hole repository layer for reinforced visible-light photocatalytic activity for degradation of refractory pollutants. Ind Eng Chem Res 60:13834–13845

Zhou C, Huang D, Xu P, Zeng G, Huang J, Shi T, Lai C, Zhang C, Cheng M, Lu Y, Duan A, Xiong W, Zhou M (2019) Efficient visible light driven degradation of sulfamethazine and tetracycline by salicylic acid modified polymeric carbon nitride via charge transfer. Chem Eng J 370:1077–1086